Journal of Chromatography A, 1218 (2011) 5216–5227

Contents lists available at ScienceDirect

Journal of Chromatography A

journal homepage: www.elsevier.com/locate/chroma

Measurement of the eddy diffusion term in chromatographic columns. I. Application to the first generation of 4.6 mm I.D. monolithic columns

Fabrice Gritti, Georges Guiochon*

Department of Chemistry, University of Tennessee, Knoxville, TN 37996-1600, USA

ARTICLE INFO

Article history:
Received 28 March 2011
Received in revised form 25 May 2011
Accepted 30 May 2011
Available online 21 June 2011

Keywords:
Column technology
Mass transfer mechanism
HETP
Monolithic column
Eddy diffusion
Trans-column effect
RPLC

ABSTRACT

The corrected heights equivalent to a theoretical plate (HETP) of three 4.6 mm I.D. monolithic Onyx-C_{18} columns (Onyx, Phenomenex, Torrance, CA) of different lengths (2.5, 5, and 10 cm) are reported for retained (toluene, naphthalene) and non-retained (uracil, caffeine) small molecules. The moments of the peak profiles were measured according to the accurate numerical integration method. Correction for the extra-column contributions was systematically applied. The peak parking method was used in order to measure the bulk diffusion coefficients of the sample molecules, their longitudinal diffusion terms, and the eddy diffusion term of the three monolithic columns. The experimental results demonstrate that the maximum efficiency was 60 000 plates/m for retained compounds. The column length has a large impact on the plate height of non-retained species. These observations were unambiguously explained by a large trans-column eddy diffusion term in the van Deemter HETP equation. This large trans-rod eddy diffusion term is due to the combination of a large trans-rod velocity bias (≃3%), a small radial dispersion coefficient in silica monolithic columns, and a poorly designed distribution and collection of the sample streamlets at the inlet and outlet of the monolithic rod. Improving the performance of large I.D. monolithic columns will require (1) a detailed knowledge of the actual flow distribution across and along these monolithic rod and (2) the design of appropriate inlet and outlet distributors designed to minimize the nefarious impact of the radial flow heterogeneity on band broadening.

1. Introduction

Monolithic columns began to be commercialized in 2000. They were based on the results of intensive research and development efforts made in the late 1980s and the 1990s on the preparation, production, and properties of continuous, bimodal porous silica [1–3]. While similar efforts were made during the same period to develop monolithic columns made of crosslinked polymers [4–6], their results were not as commercially successful. Monolithic columns differ from packed beds by the disconnection between the sizes of the porous material (the porons) and of the empty volumes available to the mobile phase flow (the throughpores). This difference has important consequences, some are well known and well advertised, others are poorly known but may explain why monolithic silica columns have met only with a modest success.

The first silica monolithic columns provided faster analyses than the conventional packed columns of the time, which used 5 μm particles, but gave a comparable efficiency. They exhibited a high sample capacity per unit adsorbent volume [7], a permeability comparable to that of 11 μm packed columns [8], and an efficiency equivalent to that of 3.5 μm packed columns [9]; they provided a much lower separation impedance than columns packed with 5 or 3.5 μm particles [10] and appeared most attractive for analytical applications in the pharmaceutical and the food industries. A review covering a decade of research and developments of monolithic columns [11] concluded that the commercial breakthrough of these new columns was slowed down by structural features inherent to their fabrication process, which cannot provide rods that are radially homogeneous [12], nor long rods and suffer from consequences of their high external porosity.

The first conclusion was confirmed by experimental results showing that silica rods are radially heterogeneous [13,14] and that there is a relative velocity difference of about 3% between the center and the wall regions of conventional monolithic rods, which explains why their HETP is so much larger (ca. 11 μm) than the average size of their porons (ca. 2 μm). It is now widely recognized that the high eddy diffusion *A* term of the van Deemter equation limits the efficiency of monolithic silica rods. Tallarek et al. [15] recently reconstructed the morphology of a 100 μm I.D. silica monolithic capillary and calculated the rate of convective-diffusive mass transport process, concluding that the trans-throughpore and the short-range inter-throughpore eddy diffusion terms are not responsible for the low efficiency reported at high flow rates, mean-

* Corresponding author. Tel.: +1 865 974 0733; fax: +1 865 974 2667.
E-mail addresses: guiochon@utk.edu, guiochon@ion.chem.utk.edu (G. Guiochon).

0021-9673/$ – see front matter © 2011 Elsevier B.V. All rights reserved.
doi:10.1016/j.chroma.2011.05.101

ing that the inherent limitation to the performance of monolith rods are due to trans-column effects and to the problem associated to the sample distribution at the rod inlet and the sample collection at the rod outlet.

The major advantages of monolithic columns, their high permeability and low mass transfer resistance, would potentially permit the rapid achievement of a high separation power by operating long columns at high velocities. A 1 m long column operated at $u_0 = 0.3$ cm/s (or a flow rate of 2.5 mL/min with a 4.6 mm I.D. rod column) would give peaks with an efficiency of 250 000 plates for butyl benzoate ($k \simeq 3$) in 333 s [9] and a back pressure of 300 bar for an acetonitrile/water mixture (55/45, v/v). Unfortunately, it is impossible to commercially produce columns much longer than 10 cm [11]. Stringing ten cm long columns would provide degraded results. As a result, the potential advantages of monolithic columns remain wasted; they found applications as second columns in 2DLC, a moderate success in the capillary format [16] or in preparative chromatography, but in an unusual format, in the radial flow configuration [17].

Finally, monolithic columns have major disadvantages due to the same reason as their high permeability: their external porosity is large, typically 0.7 *versus* 0.4 for packed beds. First, the surface area of silica per unit column volume is smaller in monoliths than in packed beds, hence retention factors are lower. Therefore, stronger equilibrium constants are required, hence weaker eluents must be used, making these columns less suitable for trace analyses due to an increased risk of thermodynamic overloading. Second, they have a low radial dispersion coefficient. This term is due to abrupt changes in the streamline direction, changes that are more frequent and strong in packed than in monolithic beds. As a result, radial mixing is slower, smaller in silica monolithic structures than in packed beds and it takes longer for the radial concentration gradients to be relaxed. Improvements of the flow distribution across and along monolithic rods are needed to increase the radial dispersion coefficient and to prepare and design monolithic columns providing an efficiency larger than 200 000 plates/m. Morphology reconstruction coupled with flow simulation is a precious tool but it requires a considerable amount of time and computer power [18,19]. The mapping of the concentration of non-retained tracer molecules in the three-dimensional bed would bring important insights on the actual dispersion of sample molecules during their migration along monolithic rods [20]. In this work, we focus on a pure chromatographic approach in order to shed new light on the trans-column eddy diffusion term of silica monolithic columns.

Regrettably, no significant progress in the performance of 4.6 mm I.D. monolithic columns has happened during the last decade. These columns are not competitive with modern columns packed with sub-2 μm [21] or recent shell particles [22–26]. It is striking that so many companies prefer to invest in new instruments able to pump eluent into columns under pressures as high as 1300 bar rather than in supporting the development of better monolithic rods.

The goal of this work was to measure the trans-rod eddy diffusion terms of three commercially available monolithic columns (Onyx-C_{18}, Phenomenex, Torrance, CA, USA) having different lengths (2.5, 5, and 10 cm) in order to accurately estimate the persistence-of-velocity length of Giddings and the diffusion distance over which a radial velocity gradient gets established. A non-invasive method previously used to study packed columns was applied [27]. It requires the measurement of the true column HETP (using the moments measured by numerical integration of the elution profiles [28]), the external porosity of the rod (using inverse size exclusion chromatography [29,30]), the longitudinal diffusion term of the van Deemter equation (using the peak parking method [31–33], and the trans-skeleton mass transfer resistance term (using the peak parking and a model of diffusion in heterogeneous media [34–37]). The external film mass transfer resistance for small molecules derived from the film penetration theory was assumed to be true [38]. The trans-throughpore and short-range inter-throughpore eddy diffusion terms were taken from the recent findings of Tallarek et al. [15] in capillary monolithic columns. We compare the trans-rod eddy diffusion terms of retained and non-retained compounds and investigate the role of the rod length on the overall efficiency of the Onyx monolithic columns.

2. Theory

2.1. Mass transfer in a monolithic column

The general HETP equation corrected for the extra-column contributions is the sum of four main independent mass transfer terms [39], accounting for the longitudinal diffusion of the analyte during its migration along the column ($H_{Long.}$), the eddy dispersion of the analyte due to a differential migration velocity across and along the column (H_{Eddy}), the resistance to mass transfer by diffusion through the porous skeleton ($H_{Skel.}$), and the mass transfer resistance between the mobile phase flowing along the throughpores and the eluent stagnant inside the mesopores of the silica skeleton (H_{Film}):

$$H = H_{Long.} + H_{Eddy} + H_{Skel.} + H_{Film} \tag{1}$$

Among these four HETP terms, only $H_{Long.}$ can be unambiguously measured by applying the peak parking method [35]. It is written:

$$H_{Long.}(u_S) = \frac{\Delta\sigma^2_{PP}}{\Delta t_p}\frac{u^2_{R,PP}}{u_S}(1+k)\epsilon_t \tag{2}$$

where $\Delta\sigma^2_{PP}$ is the variance increment measured during a peak parking period after an increment Δt_p of the peak parking time, $u_{R,PP}$ is the migration linear velocity of the analyte in the peak parking experiments, u_S is the superficial linear velocity, k is the retention factor, and ϵ_t is the total porosity of the monolithic column.

The third term in Eq. (1) or the trans-skeleton mass transfer resistance term can only be estimated provided that we assume (1) a geometry or a configuration factor for the porous skeleton and (2) a model of effective diffusion in a monolithic column. Based on scanning electron micrographs (SEM), we assume a simple cylindrical geometry for the structure of the silica monolith [38] and the simple parallel diffusion model as the effective diffusion model which gives consistent values with the effective medium theory model of Landauer [40–42]. Accordingly, $H_{Skel.}$ is written:

$$H_{Skel.} = \frac{1}{16}\frac{1}{1-\epsilon_e}\left(\frac{\delta_0}{1+\delta_0}\right)^2\frac{d^2_{skel.}}{D_{skel.}}u_S = C_{skel.}u_S \tag{3}$$

where ϵ_e is the external porosity of the monolithic column, $d_{skel.}$ is the skeleton diameter, $C_{skel.}$ is defined as the trans-skeleton mass transfer coefficient, and δ_0 is the zone retention factor given by:

$$\delta_0 = \frac{\epsilon_t}{\epsilon_e}(1+k) - 1 \tag{4}$$

$D_{skel.}$ is the sample diffusivity through the skeleton volume. According to the parallel diffusion model, the sample diffusivity in the skeleton volume is simply derived from the peak parking measurements and is written [43]:

$$D_{skel.} = \frac{1}{2}\frac{\Delta\sigma^2_{PP}}{\Delta t_p}u^2_{R,PP}(1+k)\frac{\epsilon_t}{1-\epsilon_e} - \frac{\epsilon_e}{1-\epsilon_e}\gamma_e D_m \tag{5}$$

where D_m is the bulk molecular diffusion coefficient and γ_e is the external obstruction factor generated by the monolithic structure along the chromatographic column. It was measured at 0.73

according to Ref. [15], a value consistently larger than that usually measured with packed beds ($\epsilon_e \simeq 0.60$).

The eddy dispersion term is the sum of the trans-throughpore ($H_{Channel}$), the short-range inter-throughpore (H_{Short}), and the trans-column ($H_{Trans\text{-}rod}$) eddy diffusion terms:

$$H_{Eddy} = H_{Channel} + H_{Short} + H_{Trans-rod} \quad (6)$$

Eddy diffusion in the homogeneous region of a capillary monolithic silica rod, located in the center zone, far from the wall region, was recently investigated by morphology reconstruction and simulation of convective-diffusive mass transport [15]. Tallarek et al. considered an external porosity $\epsilon_e = 0.704$, an excellent descriptor of the actual external porosity in commercially available 4.6 mm I.D. monolithic columns. The contributions of the trans-throughpore and short-range inter-throughpore velocity biases were individually obtained. They are written:

$$H_{Channel} = 0.133 \frac{d_{skel}^2}{D_m} \frac{u_S}{\epsilon_e} \quad (7)$$

and

$$H_{Short} = 1.641 \frac{u_S d_{skel}^2}{\epsilon_e D_m} \frac{1}{1 + 1.154(u_S d_{skel}/(\epsilon_e D_m))} \quad (8)$$

The trans-column eddy diffusion term $H_{Trans\text{-}rod}$ is unknown. It results from a complex combination of the radial velocity distribution, $u(x)$, the average radial dispersion coefficient, $\overline{D_r}$, and the contributions of the inlet and outlet distributors. At each end of the monolithic columns, the inlet distributor consists of a plastic frit, pierced with six equidistant holes, which are supposed to distribute the eluent stream incoming at the center of the column into six smaller equidistant streamlets emerging at about half the column radius. The reversed phenomenon, e.g. the merging of six similar streamlets into one exit stream, takes place at the column outlet. As a result, the flow profile distribution is clearly not uniform at both ends of the monolithic column, which could affect the efficiency of the whole column.

The external film mass transfer term H_{Film} accounts for the mass transfer resistance due to the thin stagnant film of eluent surrounding the porous elements of skeleton, film that the sample molecules must cross to penetrate into the porons. The driving force is the concentration difference between the eluent percolating the interstitial column volume and the stagnant eluent inside the porons. Assuming a cylindrical skeleton shape, this term writes after transformation into the Laplace domain [38,43]:

$$H_{Film} = \frac{1}{2} \frac{1}{1 - \epsilon_e} \left(\frac{\delta_0}{1 + \delta_0} \right)^2 \frac{d_{skel}}{k_f} u_S \quad (9)$$

The fraction $\frac{1}{2}$ replaces the traditional fraction $\frac{1}{3}$ for spherical particles. The film mass transfer coefficient k_f is usually calculated according to the penetration model theory [44], as suggested by Miyabe [45]. To our knowledge, this model has not yet been validated with monolithic columns. k_f is given by:

$$k_f = \sqrt{\frac{4 D_m u_S}{\epsilon_e \pi d_{skel}}} \quad (10)$$

By combining Eqs. (9) and (10), we obtain:

$$H_{Film} = \frac{1}{4\sqrt{\pi}} \frac{\epsilon_e^{1/2}}{1 - \epsilon_e} \left(\frac{\delta_0}{1 + \delta_0} \right)^2 \frac{d_{skel}^{3/2}}{D_m^{1/2}} u_S^{1/2} = C_f u_S^{1/2} \quad (11)$$

where C_f is defined as the external film plate height coefficient.

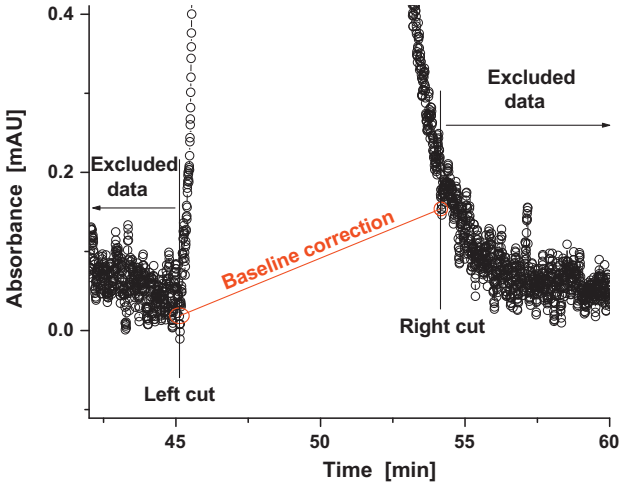

Fig. 1. Peak processing for the determination of the first and second central moments. The graphs show a zoom to the base of a recorded peak profile. The left and right cut abscissa are selected when the slopes of the decreasing branches of the recorded peak become positive for the first time. All the data points recorded before the left cut-off abscissa and after the right cut-off abscissa are eliminated and the signal is corrected for baseline linear drift (red solid line) before numerical integration. (For interpretation of the references to color in this figure legend, the reader is referred to the web version of the article.)

2.2. Determination of the true chromatographic HETP

The first and second central moments of the extra-column and overall (system + column) peak profiles were measured by numerical integration of the full concentration profiles. Prior to any measurement, each elution profile was treated according to the procedure described in Fig. 1. First, a fraction of the data points at the left and at the right of the peak are excluded from the numerical calculations. The left and right cuts are determined as the times when the average slope of the signal decay measured over $N/200$ consecutive points is larger or equal to zero. N is the number of points which describe the data profile between the left and right cuts. In a second step, the peak profile is corrected for a linear baseline drift joining the left and right cut points. Finally, the first and second central moments of the concentration profiles were calculated in an Excel spread-sheet using the selected data points. They are given by:

$$\mu_1 = \frac{\sum_{i=1}^{i=N-1} (C_i + C_{i+1})(t_i + t_{i+1})}{2 \sum_{i=1}^{i=N-1} C_i + C_{i+1}} \quad (12)$$

$$\mu'_2 = \frac{\sum_{i=1}^{i=N-1} (C_i + C_{i+1}(((t_i + t_{i+1})/2) - \mu_1))^2}{\sum_{i=1}^{i=N-1} C_i + C_{i+1}} \quad (13)$$

The corrected HETP, H, is then given by:

$$H = L \frac{\mu'_2 - \mu'_{2,ex}}{(\mu_1 - \mu_{1,ex})^2} \quad (14)$$

where L is the column length and $\mu_{1,ex}$ and $\mu'_{2,ex}$ are the first and the second central moments of the corresponding extra-column band profiles. As demonstrated in a previous paper, this method is correct and should replace the incorrect, approximate, and inaccu-

rate method consisting in measuring the correction from the peak widths at mid-height [28]. The precision of the H data is given by

$$\left|\frac{\Delta H}{H}\right| = \left|\frac{\Delta\mu'_2}{\mu'_2}\right| \left(\frac{\mu'_2 + \mu'_{2,ex}}{\mu'_2 - \mu'_{2,ex}}\right) + 2\left|\frac{\Delta\mu_1}{\mu_1}\right| \left(\frac{\mu_1 + \mu_{1,ex}}{\mu_1 - \mu_{1,ex}}\right) \quad (15)$$

The second and first moments of the tracer peak, μ'_2 and μ_1, were measured for five successive injections, first with the chromatographic column, then with a zero-volume connector fitted to the instrument. The relative errors made on the first moments are 0.3, 0.7, and 4% at flow rates of 0.04, 0.4, and 4 mL/min, respectively. The relative error made on the second central moments is equal to 3% when 1 μL are injected from a 20 μL loop. This excellent level of repeatability of the injection system of the 1290 Infinity system is what permits the excellent precision of the H measurements. The poor reproducibility of the first moment at the highest flow rate is related to the electronic asynchronization between the moments when the injection valve is actuated and when the zero time is recorded. Actually, the precision of the numerical integration method to measure the second central moment depends essentially on the left and right cut-off abscissa. The 3% precision was obtained when these abscissa were identical for all five injections. However, when the flow rate is changed, so are the cut-off abscissa and the precision of the peak variance plotted as a function of the flow rate may seem lesser. Yet, the integration approach provides the only accurate HETP data that the analyst can obtain [28]. It is much better than those provided by inaccurate, approximate approaches such as the half-height peak width and/or the peak fitting methods.

Accordingly, if the extra-column contributions were to be negligible, the largest random error would be 3.6, 4.4, and 12% at flow rates of 0.04, 0.4, and 4 mL/min. This is typically the case of results obtained for large volume and poorly efficient columns such as the 4.6 mm I.D. silica-C_{18} monolithic columns used in this work (see kinetic performance later in Section 4).

3. Experimental

3.1. Chemicals

The mobile phase was a mixture of acetonitrile and water (55/45, v/v). Tetrahydrofuran was also used as the eluent for inverse size-exclusion chromatography (ISEC) measurements. All these pure eluents were HPLC grade from Fisher Scientific (Fair Lawn, NJ, USA). The mobile phases were filtered before use on a surfactant-free cellulose acetate filter membrane, 0.2 μm pore size (Suwannee, GA, USA). Eleven polystyrene standards (MW = 590, 1100, 3680, 6400, 13 200, 31 600, 90 000, 171 000, 560 900, 900 000, and 1 877 000) were used to acquire ISEC data. They were purchased from Phenomenex (Torrance, CA, USA). The low molecular weight compounds used in this work were uracil, caffeine, toluene, and naphthalene with a minimum purity of 99% (Fair Lawn, NJ, USA).

3.2. Apparatus

The 1290 Infinity HPLC system (Agilent Technologies, Waldbroen, Germany) liquid chromatograph used in this work includes a 1290 Infinity Binary Pump with Solvent Selection Valves and a programmable auto-sampler. The injection volume was set at 1 μL and was drawn into one end of the 20 μL injection loop. The instrument is equipped with a two-compartment oven and a multi-diode array UV–vis detection system. The system is controlled by the Chemstation software. The sample trajectory in the equipment involves the successive passage of the sample band through

- A 20 μL injection loop attached to the injection needle. The design of the injection system is such that the volume of sample drawn into the loop is the volume of sample injected into the column.
- A small volume needle seat capillary (115 μm I.D., 100 mm long), ≃1.0 μL, located between the injection needle and the injection valve. The total volume of the grooves and connection ports in the valve is around 1.2 μL.
- Two connector capillaries (red tubing), with 120 μm I.D., the first being 220 mm long (before the heat exchanger) and the second 220 mm long (after the column and before the detector cell). Their total volume is 5.0 μL.
- A small volume detector cell, 0.8 μL, 10 mm path.

The extrapolation to a zero flow rate of the extra-column volume measured from 1 μL injections of uracil, caffeine, toluene, and naphthalene tracers in the range of flow rates between 0.1 and 4.0 mL/min provides an average extra-column volume of 9.7 μL. According to the dimensions cited above, we should expect a volume of 0.5 (injection volume) + 1.0 (needle seat capillary) + 1.2 (injection valve) + 5 (inlet and outlet capillaries) + 0.4 (detector cell) = 8.1 μL. Given the wide range of the specifications (±20%) for the inner diameter of the connecting capillary tubes, these two values are in good agreement. We measured an offset time of about 0.05 s between the moments when the zero time is recorded and when the sample leaves the injection needle.

The extra-column peak variances increase from 3 μL^2 at 0.1 mL/min to 12 μL^2 at 4 mL/min.

3.3. Columns

Three 4.6 mm I.D. Onyx monolithic columns of different lengths (25, 50, and 100 mm) were purchased from Phenomenex (Torrance, CA, USA). They were not used before this work and they were stored in a mixture of acetonitrile and water (60/40, v/v). The different characteristics of these columns are listed in Table 1. The modified silica-C_{18} surface areas were all endcapped according to a proprietary process.

The 100 mm × 4.6 mm I.D. column packed with 1.9 μm nonporous silica particles was a generous gift from Phenomenex (Torrance, CA, USA).

3.4. Peak parking (PP) experiments

The PP method was used to measure the longitudinal diffusion HETP terms (B/u_S) of the monolithic columns studied and the effective diffusivities ($D_{skel.}$) of the samples through their porous skeleton. This technique was pioneered by Knox in gas [46] and liquid chromatography [31] and was recently used to measure the internal obstruction factor of porous silica-C_{18} particles [32] and the bulk diffusion coefficients of sample molecules in the liquid mobile phase [47,48].

In the PP experiments reported, 1 μL of a dilute sample solution (<0.5 g/L) was injected at a constant flow rate, which was set depending on the retention factor k of the sample, at 0.15 mL/min with the non-retained compounds uracil and caffeine and at 0.40 mL/min with the retained compounds, toluene and naphthalene. The column was eluted during the time necessary for the sample to reach about half the length of the monolithic column. Then, the flow is abruptly stopped and the sample left free to diffuse along the column bed during a certain time. This parking time was successively set at 1, 60, 120, 180, and 240 min. The slope of the plot of the elution peak variance *versus* the peak parking time, $\Delta\sigma^2_{PP}/\Delta t_p$,provides a direct measure of the longitudinal diffusion coefficient ($H_{Long.}$, Eq. (2)) and an estimate of the sample diffusivity through the porous skeleton ($D_{skel.}$, Eq. (5)).

Table 1
Characteristics of the three research samples according to the manufacturer and our measurements.

	Onyx monolithic columns		
Batch number	8278-47	8941-16	8191-44
Serial number	080710-42	070730-98	080620-54
Rod dimension	25 mm × 4.6 mm	50 mm × 4.6 mm	100 mm × 4.6 mm
Onyx monolith			
Silica type	High purity	High purity	High purity
Average throughpore size [μm]	2.0	2.0	2.0
Average skeleton size [a] [μm]	0.8	0.8	0.8
Mesopore size [Å]	130	130	130
Specific surface area [m^2/g]	300	300	300
C_{18}-bonded Onyx			
ϵ_e [b]	0.72	0.72	0.71
ϵ_t [c]	0.84	0.83	0.82
ϵ_{skel} [d]	0.43	0.39	0.38

[a] Indirectly measured from ISEC.
[b] Measured from ISEC.
[c] Measured from the elution volume of uracil.
[d] Calculated from $\epsilon_{skel} = (\epsilon_t - \epsilon_e)/(1 - \epsilon_e)$.

3.5. Measurement of the bulk diffusion coefficients D_m

The diffusion coefficients of uracil, caffeine, toluene, and naphthalene were measured with the peak parking method, using a 100 mm × 4.6 mm column packed with solid, non-porous silica particles (1.9 μm). The diffusion coefficient $D_m(T)$ at temperature T is obtained from the peak parking data measured at temperature T_{PP} by [35]:

$$D_m(T) = \frac{1}{2\gamma_e} \frac{\Delta\sigma^2_{PP}(T_{PP})}{\Delta t_p} \frac{L^2}{t_R^2} \frac{T}{T_{PP}} \frac{\eta(T_{PP})}{\eta(T)} \quad (16)$$

where γ_e is the external obstruction factor of the column packed with solid particles, L is the column length, t_R is the retention time of the compound with no flow interruption, and $\eta(T)$ and $\eta(T_{PP})$ are the eluent viscosities at temperatures T and T_{PP}. γ_e was measured from the peak parking experiments using thiourea, a compound having a precisely known diffusion coefficient in pure water, at T = 298.15 K, $D_m = 1.33 \times 10^{-5}$ cm^2/s [49,50]. Accordingly, we measured $\gamma_e = 0.65$.

The flow rate was fixed at 0.4 mL/min. The peak parking times were set at 1, 60, 120, 180, and 240 min. The temperature profile T_{PP} was recorded by the instrument during the whole PP experiments. Due to slight temperature variations overnight (±1 K during a 10 h sequence run), T_{PP} was taken as the mean of the five average temperatures recorded during each arrested flow experiment. All the experimental results and the diffusion coefficients are given in Table 2 and compared to the values predicted by the Wilke and Chang correlation [51]. Note that the relative errors made by using the Wilke and Chang correlation are +13% (uracil), −6% (caffeine), −65% (toluene), and −35% (naphthalene). Whereas the estimates of the diffusion coefficients are acceptable for uracil and caffeine, they are not so for the apolar samples, toluene and naphthalene. The direct measurement of the true diffusion coefficients is then mandatory whenever accurate results are needed. For the sake of comparison, Carr and Li [52] measured for the diffusion coefficient of toluene values of 1.13×10^{-5} and 1.71×10^{-5} cm^2/s at 303 K for acetonitrile concentrations of 50 and 60%, respectively. We measured values of 1.36×10^{-5} cm^2/s at 300 K, for an acetonitrile concentration of 55%, which are in excellent agreement with the experimental data of Carr and Li.

3.6. HETP plots

For all samples, the same sequence of flow rate was 0.1, 0.2, 0.3, 0.4, 0.6, 0.8, 1.0, 1.25, 1.50, 1.75, 2.0, 2.5, 3.0, 3.5, and 4.0 mL/min. The sampling rate was adjusted to 5, 10, 20, 20, 20, 40, 40, 80, 80, 80, 80, 160, 160, 160, and 160 Hz, respectively, in order to record peak profiles with a comparable number of data points at all flow rates. One μL of each sample solutions (concentration <0.5 g/L) was injected and the chromatograms were recorded at wavelengths of 265, 265, 225, and 265 nm for uracil, caffeine, toluene, and naphthalene, respectively. For all samples a constant bandwidth of 4 nm was selected. The temperature was set by the laboratory air-conditioner at 300 ± 1 K.

3.7. ISEC experiments

The ISEC experiments were carried out with neat THF as the eluent. Twelve polystyrene standards were used with molecular weight between 100 and 2 millions Dalton. This covers a wide range of molecular sizes between 4 and 950 Å. The flow rate was set at 0.15 mL/min with the 4.6 × 25 mm Onyx-C_{18} monolithic column and at 0.30 mL/min for both the 50 and 100 mm long columns. The external porosity was determined from the extrapolated elution volumes of the exclusion branches (see red solid straight lines in Fig. 2A–C) to a molecular radius of zero divided by the PEEK tube volume (0.416, 0.813, and 1.662 cm^3). The results are listed in Table 1. The average thickness of the skeleton diameter ($d_{skel.}$ = 0.8 μm) was estimated from the average diameter of the

Table 2
Measurement of the diffusion coefficients of uracil, caffeine, toluene, and naphthalene in a mixture of acetonitrile and water (55/45, v/v) at T = 300 K using a 100 mm × 4.6 mm column packed with 1.9 μm non-porous silica particles. The external obstruction factor of this column was measured from the known diffusion coefficient of thiourea ($D_m = 1.33 \times 10^{-5}$ cm^2/s at T = 298.15 K) and is equal to $\gamma_e = 0.65$.

Compound	Temperature Peak parking [K]	Eluent	Viscosity eluent [cP]	$u_{R,PP}$ [cm/s]	$\Delta\sigma^2_{PP}/\Delta t_P$ [ms]	D_m [cm^2/s] Peak parking	D_m [cm^2/s] Wilke and Chang
Uracil	293.55	CH_3CN/H_2O (55/45, v/v)	0.835	9.28×10^{-2}	1.44	9.54×10^{-6}	1.09×10^{-5}
Caffeine	293.55	CH_3CN/H_2O (55/45, v/v)	0.835	9.25×10^{-2}	1.21	7.96×10^{-6}	7.53×10^{-6}
Toluene	293.15	CH_3CN/H_2O (55/45, v/v)	0.855	9.28×10^{-2}	2.05	1.36×10^{-5}	9.70×10^{-6}
Naphthalene	293.15	CH_3CN/H_2O (55/45, v/v)	0.855	9.28×10^{-2}	1.70	1.13×10^{-5}	8.40×10^{-6}

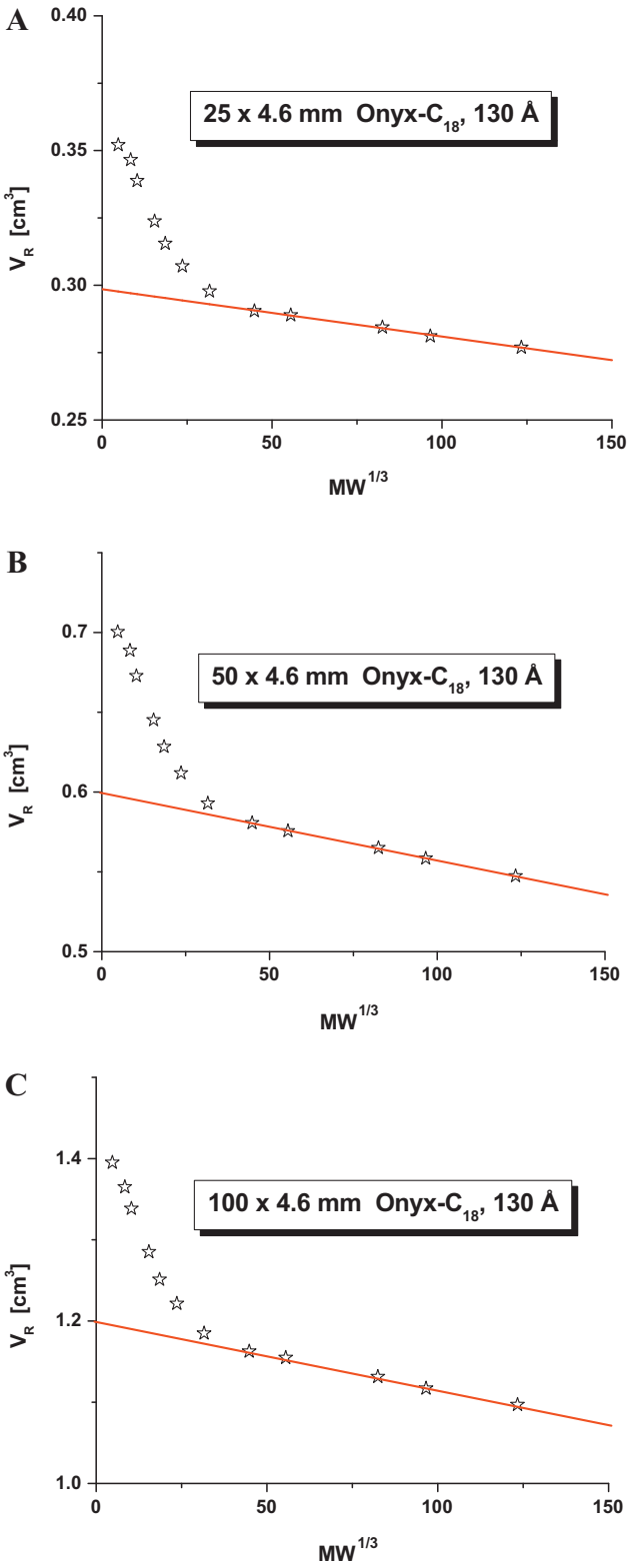

Fig. 2. ISEC plots (elution volume of the polystyrene standards *versus* the cubic root of the molecular weight) measured with the 25 mm (A), 50 mm (B), and 100 mm (C) × 4.6 mm I.D. Onyx-C_{18} monolithic columns. The external porosity of all three monolithic rods is $\epsilon_e = 0.72$.

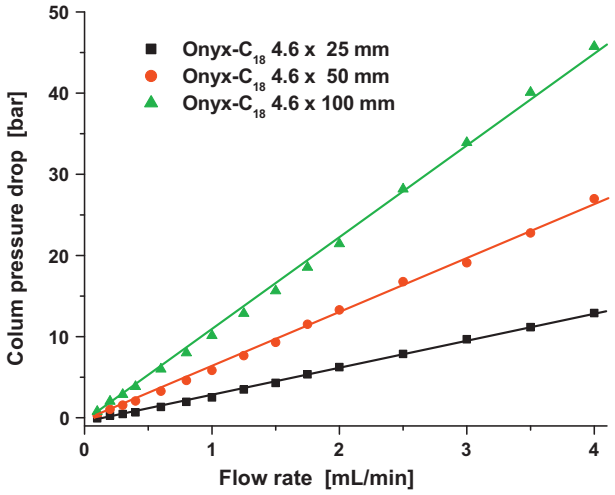

Fig. 3. Column pressure drops measured on the three Onyx-C_{18} monolithic columns as a function of the applied flow rate. $T = 300$ K. Eluent: acetonitrile/water (55/45, v/v). The pressures were corrected for the 1290 Infinity system contributions.

throughpores ($d_{throughpores} = 2.0\,\mu m$) and the external porosity of the monolithic column ($\epsilon_e = 0.72$)

$$d_{skel.} = \frac{1-\epsilon_e}{\epsilon_e} d_{throughpores} \quad (17)$$

Eq. (17) is exact for unidimensional systems such as those having a flat wall, which we assumed as a first simple approximation. If we assume a cylindrical skeleton, we would find $d_{skel.} = 1.2\,\mu m$. Most likely, this underestimates the average skeleton size. Because the monolithic structure results from randomly interconnected volumes of silica with no clearly defined shape, we estimate d_{skel} merely from the simple Eq. (17). The manufacturer provided estimates of the skeleton thickness at around 1 μm for a domain size of 3 μm, with no further precision. However, because, in this work we study low molecular weight compounds, the solid-liquid mass transfer resistance term is negligible compared to the eddy diffusion term. Therefore, the error made on the estimate of the average skeleton diameter has no significant effect on the value of the eddy diffusion term of a monolithic column.

4. Results and discussion

In the first part of this work, we measured the permeability of the three Onyx columns and determined the equivalent particle size that would give the same pressure drops. The first monolithic columns commercialized had an average domain size (skeleton + throughpore sizes) of 3.5 μm and the same permeability as columns packed with 11 μm particles [8]. In a second part, we accurately measured the overall kinetic performance of these columns for non-retained and retained compounds. Finally, in the last part, we combine the results of all the experiments described in the experimental section (HETP data, PP data, and ISEC data) in order to measure the contribution of eddy diffusion to the overall HETP.

4.1. Permeability of the monolithic columns

The pressure drops along the monolithic columns were measured by subtracting the system pressure drop (measured in the absence of column) to the total pressure drop (measured in the presence of a monolithic column). The plots of these corrected pressure drops *versus* the applied flow rate are shown in Fig. 3 for the three monolithic columns, at a constant temperature of 300 K. The viscosity of the eluent (acetonitrile/water, 55/45, v/v) at this

temperature is $\eta = 0.721$ cP. The pressure drop, ΔP, is given by the general permeability equation [39]:

$$\Delta P = \frac{\eta L}{\pi R_c^2 k_0} F_v \tag{18}$$

From the best slopes of the nearly linear plots in Fig. 3, we can estimate the specific permeability, k_0, of each monolithic column, knowing the internal radius of the PEEK tube ($R_c = 0.23$ cm). They are 5.35, 5.34, and 6.24×10^{-14} m^2 for columns with lengths of 2.5, 5, and 10 cm, respectively. The permeability of chromatographic columns packed with spherical particles is given by the Kozeny–Carman relationship and:

$$k_0 = \frac{\epsilon_e^3 d_p^2}{K_c(1-\epsilon_e)^2} \tag{19}$$

where ϵ_e is usually of the order of 0.40 and the Kozeny–Carman constant, K_c, is equal to 180. Columns packed with particles having an average diameter of 7.4 to 8.0 μm and having the same length as the Onyx columns would provide the same permeability.

4.2. Performance of the monolithic columns

According to the manufacturer (Certificate of Quality Assurance), the efficiencies of the 2.5, 5, and 10 cm long Onyx-C_{18} columns are 72 280, 78 240, and 84 200 plates/m at a flow rate of 2 mL/min, at ambient temperature, with an aqueous mobile phase containing 60% of acetonitrile in volume, and progesterone ($k = 1.9$) as the analyte. Under the same experimental conditions, these efficiencies drop to 18 520, 28 680, and 47 290 plates/m for a non-retained compound, thiourea. However, nothing was mentioned in the report on how these plate counts were measured.

Fig. 4A–C shows the corrected plate heights, H (in μm), of the three columns as a function of the superficial linear velocity (in cm/s), u_S. For the sake of comparison with the manufacturer's report, we measured the plate counts of the uracil ($k \simeq 0$) and toluene peaks ($k = 1.9$) at 2 mL/min. For uracil, the values found, 20 814 (+12%), 36 237 (+26%), and 42 649 (−10%), are in good agreement with those reported by the manufacturer for thiourea. In contrast, even after correction for the extra-column contributions, they are only 48 646 (−33%), 51 180 (−35%), and 47 671 (−43%) for toluene, or about two-third those reported by the manufacturer. The differences are even larger for the efficiencies measured with naphthalene (−50% to −60%). This is probably related to the method used by the manufacturer to measure these efficiencies. The method that we use is accurate (see earlier, Section 2.2). The column is brand new and has never been used before this work, so no deterioration of the column can be suspected. Finally, progesterone is not supposed to tail less than apolar toluene.

In order to clarify the origin of this difference, we measured the efficiency of the most retained of our probe compounds, naphthalene, on the three Onyx column by using the half-height peak width method. As shown earlier [28], this method provides an overestimate of the true column efficiency, because it neglects the influence of the peak tailing. We found N values of 2653 ($L = 25$ mm), 5298 ($L = 50$ mm), and 10 340 (100 mm) whereas the Certificate of Quality Assurance reported values of 2648 ($L = 25$ mm), 4959 ($L = 50$ mm), and 10 270 (100 mm). Both sets of value are in excellent agreement, confirming our earlier results [28]. Obviously, the efficiencies reported by the manufacturer are obtained with the half-height peak width method, which is particularly regrettable considering the important tailing of their probe compound.

We also measured the US Pharmacopeia (USP) tailing factor at 5% of the peak height. The manufacturer reported values of 1.56, 1.42, and 1.42 for thiourea and 1.34, 1.44, and 1.48 for progesterone. However, we measured USP tailing factors at the same flow

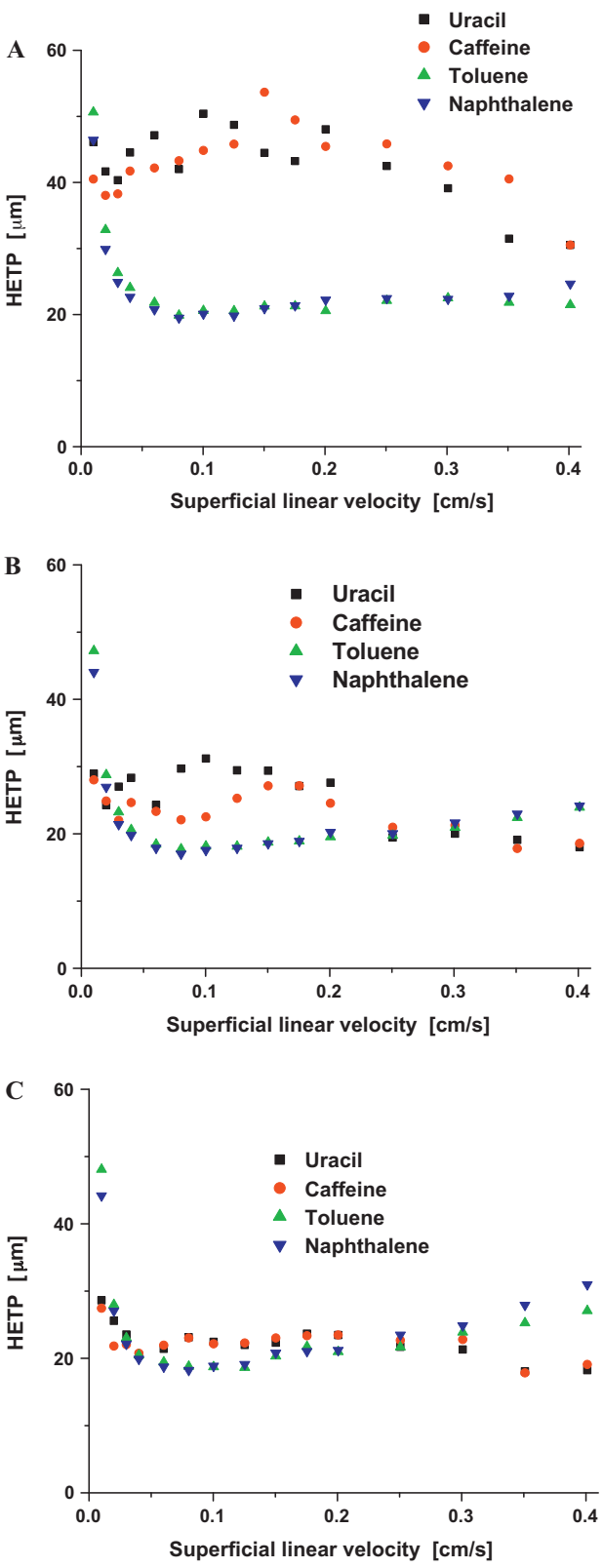

Fig. 4. Plots of the corrected HETPs of uracil, caffeine, toluene, and naphthalene on the 25 mm (A), 50 mm (B), and 100 mm (C) × 4.6 mm I.D. Onyx-C_{18} monolithic columns. Note the striking difference between the data for retained and non-retained samples.

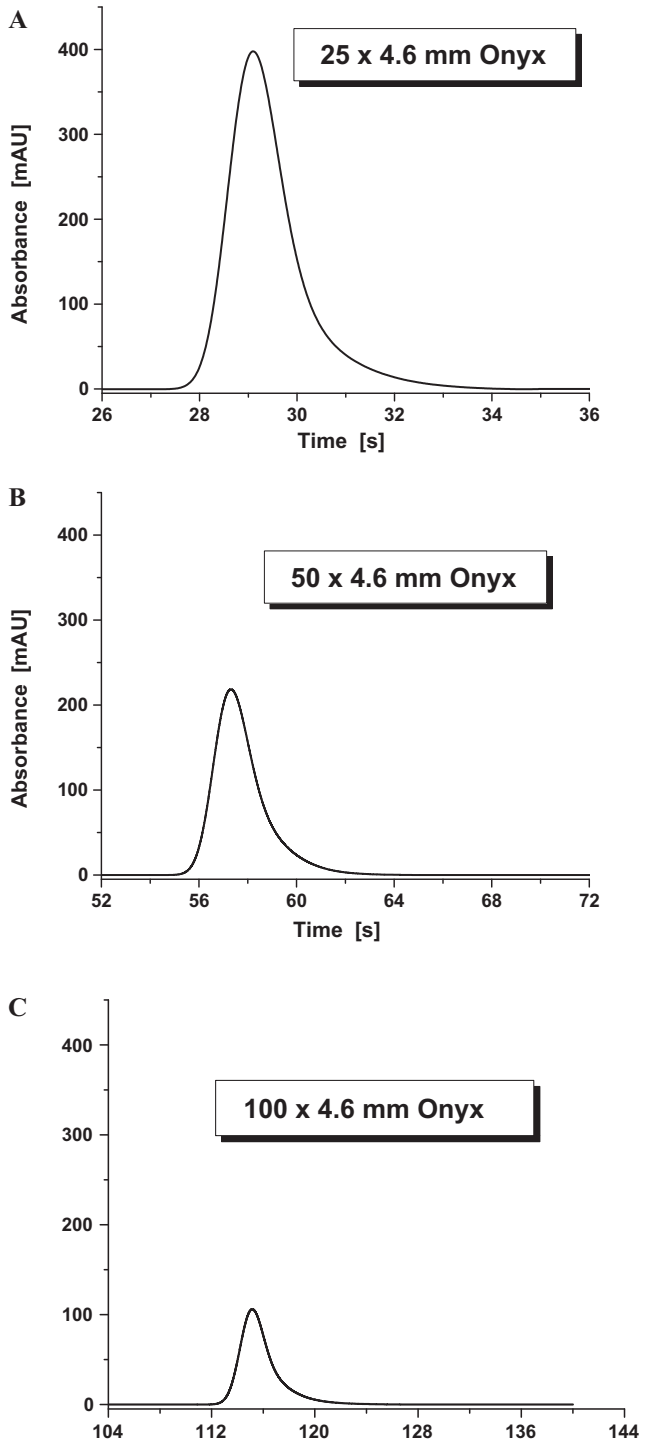

Fig. 5. Example of recorded peak profiles of a small compound (toluene) on the 25 mm (A), 50 mm (B), and 100 mm (C) × 4.6 mm I.D. Onyx-C_{18} monolithic columns. Flow rate: 2 mL/min. Injection volume: 1 μL. T = 300 K. Mobile phase: acetonitrile/water (55/45, v/v). Note the systematic peak tailing which explains the relatively poor efficiency of these columns.

rate of 2.17, 1.82, and 2.34 for uracil and of 1.62, 1.60, and 1.62 for toluene. These values are 40% (for thiourea) and 13% (for naphthalene) larger than those reported by the manufacturer. Fig. 5 illustrates the importance of the tailing of the toluene peak on the three Onyx-C_{18} columns.

Note also that the smallest total peak variance (165 μL^2) measured for uracil on the 25 mm Onyx column was recorded at the fastest flow rate, 4 mL/min. In contrast, for toluene it was recorded at a flow rate of only 0.8 mL/min (765 μL^2). The corresponding contributions of the extra-column peak variances were 11.5 and 8.7 μL^2, accounting for 7.0 and 1.1% of the total peak variance of uracil and toluene, respectively. This proves that the peak tailing observed with toluene cannot be attributed to the extra-column band broadening. The distribution of the sample band at the inlet of the monolithic rod, the trans-column axial velocity distribution, and the merging of the eluent streamlets at the outlet of the column are necessarily responsible for the relatively poor efficiency measured for the retained compounds (toluene and naphthalene). Undoubtedly, the relatively poor performance of these three Onyx columns is inherent to the particular design of the rod monolithic columns.

Unlike in packed columns ($\epsilon_e \simeq 0.37$), radial mixing in monolithic columns is relatively small because their external porosity is twice as large ($\epsilon_e \simeq 0.72$) and the eluent streamlines are less tortuous in monolithic ($\gamma_e \simeq 0.75$) than in packed columns ($\gamma_e \simeq 0.60$). The porous silica skeleton accounts for only 28% of the column volume and contributes less to homogenize the radial concentration gradients than a bed of packed spherical particles. As the retention factor increases and so does the residence time of the sample band inside the column, the USP tailing factor usually decreases for packed columns because the radial velocity gradients are rapidly relaxed [53,54]. This justifies the better true efficiencies measured with strongly than with poorly retained samples. Fig. 4A–C also shows that the HETPs of both toluene and naphthalene do not vary significantly from the 25 to the 50 or the 100 mm long monolithic column. A nearly constant minimum HETP of 17–19 μm is measured, a minimum plate height far above the values of 9–10 μm claimed in the Certificate of Quality Assurance. In contrast, the longer the column, the lower the minimum plate height of the non-retained compounds (uracil and caffeine); it decreases from 30.5 (25 mm long column) to 18 μm (50 and 100 mm long columns). Interestingly, this minimum was observed at the highest flow rate of 4 mL/min, suggesting that at a higher flow rate, the radial dispersion coefficients in the monolithic rods could possibly increase, speeding up the relaxation of radial concentration gradients by means of a convective dispersion process. This confirms that the C term of monolithic columns is rather small, due to the small thickness of the porous skeleton (≃0.8 μm), and that the mass transfer of weakly retained compounds at high flow rate is controlled by eddy diffusion.

These observations led us to measure the contributions of longitudinal diffusion and the trans-skeleton mass transfer resistance terms and combine them to the overall experimental HETP, in order to extract the contribution of the eddy diffusion HETP term to the overall HETP of the monolithic columns.

4.3. Eddy diffusion in monolithic columns

In this section we apply a method that we recently introduced [35], aiming at isolating the eddy diffusion term of chromatographic columns. This method was successfully applied to explain the difference between the A terms of columns packed with fully and superficially porous spherical particles [27,55]. In the theory Section, we provided a quantitative explanation of how the coefficients B, C_{skel}, and C_f are derived from experimental data (B and $C_{skel.}$) and from an available model (C_f). Table 3 summarizes all these results. The eddy diffusion term is simply measured according to:

$$H_{eddy} = H - \frac{B}{u_S} - C_{skel.}u_S - C_f u_S^{1/2} \quad (20)$$

The results are shown in Fig. 6A–C. As explained earlier, the error made on the skeleton diameter has nearly no influence on these representations. If $d_{skel.}$ be equal to 1.2 μm, the largest relative error would be only 0.2%. Clearly, the eddy diffusion term strongly

Table 3
B, C_p, and C_f coefficients measured from the peak parking method at $T = 300$ K for four small molecules in three monolithic columns having different lengths (25, 50, and 100 mm). The viscosity of the eluent is equal to 0.723 cP.

Compound	Column length [mm]	Eluent	Retention factor	Bulk diffusion coefficient	Longitudinal diffusion coefficient	Trans-skeleton mass transfer resistance	External film mass transfer resistance
			k	D_m [cm^2/s] Peak parking	B [cm^2/s] Peak parking	C_{sket} [μs] Peak parking + diffusion model	C_f [cm$^{1/2}$ s$^{1/2}$] Penetration theory
Uracil	25	CH_3CN/H_2O (55/45, v/v)	0.000	1.12×10^{-5}	1.58×10^{-5}	4.41	1.99×10^{-6}
	50		0.000		1.54×10^{-5}	3.85	1.58×10^{-6}
	100		0.000		1.59×10^{-5}	2.94	1.38×10^{-6}
Caffeine	25	CH_3CN/H_2O (55/45, v/v)	0.063	9.38×10^{-6}	1.54×10^{-5}	5.66	3.91×10^{-6}
	50		0.066		1.63×10^{-5}	4.26	3.42×10^{-6}
	100		0.068		1.50×10^{-5}	4.95	3.19×10^{-6}
Toluene	25	CH_3CN/H_2O (55/45, v/v)	1.787	1.93×10^{-5}	4.75×10^{-5}	14.1	33.2×10^{-6}
	50		1.800		4.57×10^{-5}	15.0	33.2×10^{-6}
	100		1.846		4.62×10^{-5}	14.8	33.3×10^{-6}
Naphthalene	25	CH_3CN/H_2O (55/45, v/v)	2.477	1.37×10^{-5}	4.37×10^{-5}	15.5	46.8×10^{-6}
	50		2.488		4.28×10^{-5}	15.9	46.9×10^{-6}
	100		2.559		4.36×10^{-5}	15.5	47.0×10^{-6}

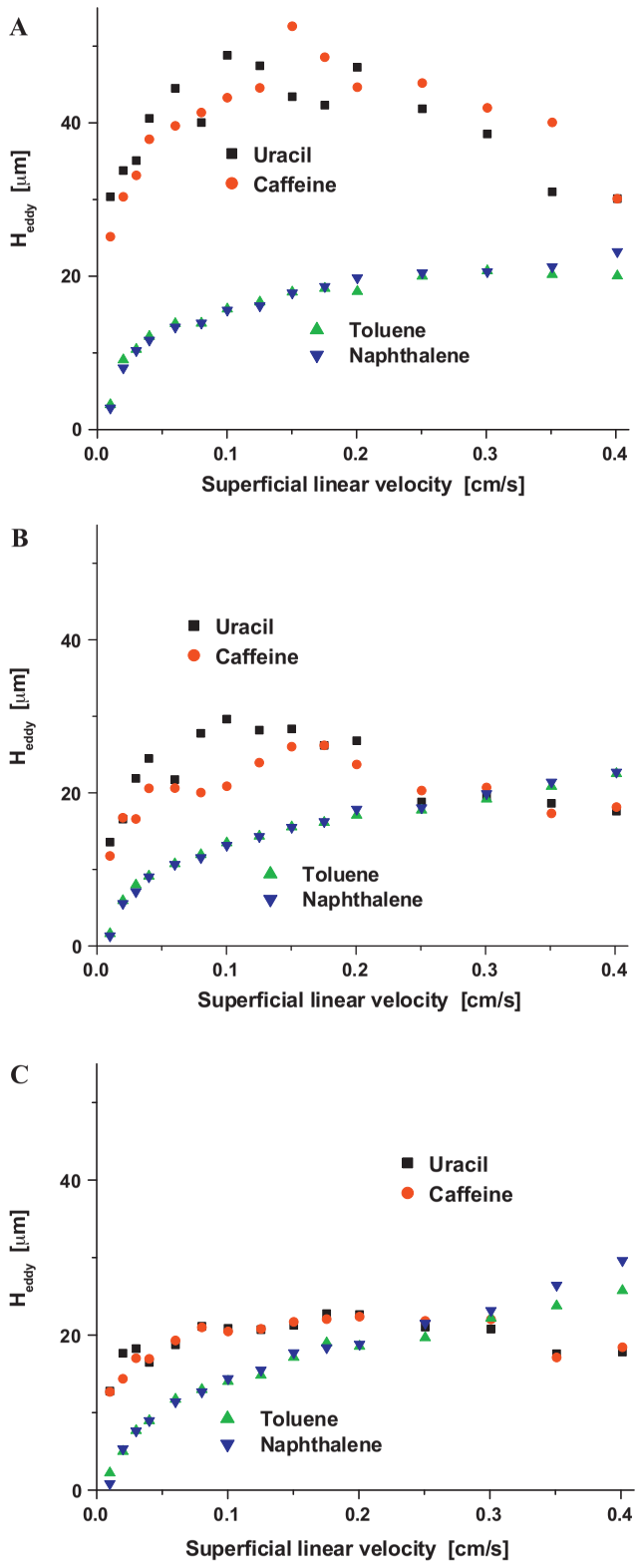

Fig. 6. Plots of the estimated total eddy diffusion terms of uracil, caffeine, toluene, and naphthalene on the 25 mm (A), 50 mm (B), and 100 mm (C) × 4.6 mm I.D. Onyx-C_{18} monolithic columns versus the superficial velocity. Note the difference between retained and non-retained compounds.

depends on the retention of the sample, as explained in the previous section. This is particularly true when the length of the monolithic rod decreases, e.g., when the amount of time during which the sample molecules can disperse radially decreases. As previously demonstrated [53,54], such a large difference between the eddy diffusion terms of retained and non-retained compounds always mirror the existence of significant trans-column velocity biases. For the sake of comparison, the trans-channel (Eq. (7)) and the short-range interchannel eddy diffusion terms (Eq. (8)) at a superficial linear velocity of 0.4 cm/s are 0.5 and 1.5 μm, respectively. Clearly, these eddy diffusion terms have only a marginal impact on the overall eddy diffusion in a 4.6 mm I.D. monolithic column. This is confirmed by recent independent results on a capillary monolithic column [15]. Our accurate measurements showed that the total eddy diffusion term at a superficial velocity of 0.4 cm/s (4 mL/min) is around 20 μm. Fig. 6C shows the typical trans-column eddy diffusion terms of non-retained and retained compounds in the 100 mm long Onyx column. The large diffusivity of toluene and naphthalene across the porous skeleton and their long residence time inside the column (see the difference between their B coefficients in Table 3) permit a faster release of the radial velocity gradients at low velocities [54]. Interestingly, the eddy diffusion terms of the two non-retained samples, uracil and caffeine, decrease at high flow velocities. The most plausible explanation is the rapid increase of the average radial dispersion coefficient, $\overline{D_r}$, with increasing flow rate due to enhanced convective sample dispersion. This phenomenon is particularly obvious with the shortest monolithic column on which the USP tailing factor of uracil decreases from 2.2 at 0.4 mL/min to 1.8 at 4 mL/min. In contrast, the USP tailing factor of toluene barely changes from 1.63 to 1.57.

The trans-column eddy diffusion term is then responsible for the relatively poor performance of the Onyx monolithic columns. The general expression of the trans-column eddy diffusion term is written [39]:

$$H_{Trans-rod} = \frac{1}{(1/H_{Flow}) + (1/H_{Diffusion})} \quad (21)$$

H_{Flow} is the hypothetical trans-column eddy diffusion plate height in the absence of radial diffusion in the monolithic rod [39,54]:

$$H_{Flow} = \omega_\beta^2 \omega_\lambda d_{skel.} \quad (22)$$

where ω_β is the ratio of the differences between the extreme velocity across the column diameter to the average velocity (u_S/ϵ_e) and $\omega_\lambda d_{skel.}$ is the persistence-of-velocity length.

In fact, the concentration gradients across the column are relaxed by dispersion of the sample molecules. The plate height $H_{Diffusion}$ is written [39]:

$$H_{Diffusion} = \frac{\omega_\beta^2 \omega_\alpha^2}{2} \frac{d_{skel.}^2 u_S}{(1+k)\epsilon_t \overline{D_r}} \quad (23)$$

where $\omega_\alpha d_{skel.}$ is the distance along which a molecule should diffuse to move from one extreme velocity to the next and $\overline{D_r}$ is the average radial dispersion coefficient, which is expressed as the sum of a diffusive and a convective diffusion coefficient [56,57]:

$$\overline{D_r} = \frac{1}{2}\left[\frac{B}{(1+k)\epsilon_t} + \gamma_r u_S d_{skel.}\right] \quad (24)$$

where γ_r is equal to 0.32 for columns packed with spherical particles [58]. Most likely, the value of γ_r for monolithic columns is smaller than 0.32 because the external obstruction factor is smaller (0.73 *versus* 0.6). We assume $\gamma_r = 0.20$ for monolithic silica rods.

The results of a multi-linear regression analysis (see the comparison between our experimental data and the predictions resulting from Giddings results in Fig. 7) provide estimates of the physical parameters ω_λ and ω_α that minimize the distance between the experimental data and the values calculated with Eq. (21), $\omega_\beta^2\omega_\lambda = 25$ and 40 and $\omega_\beta^2\omega_\alpha^2/2 = 534$ and 97 for uracil and for toluene, respectively.

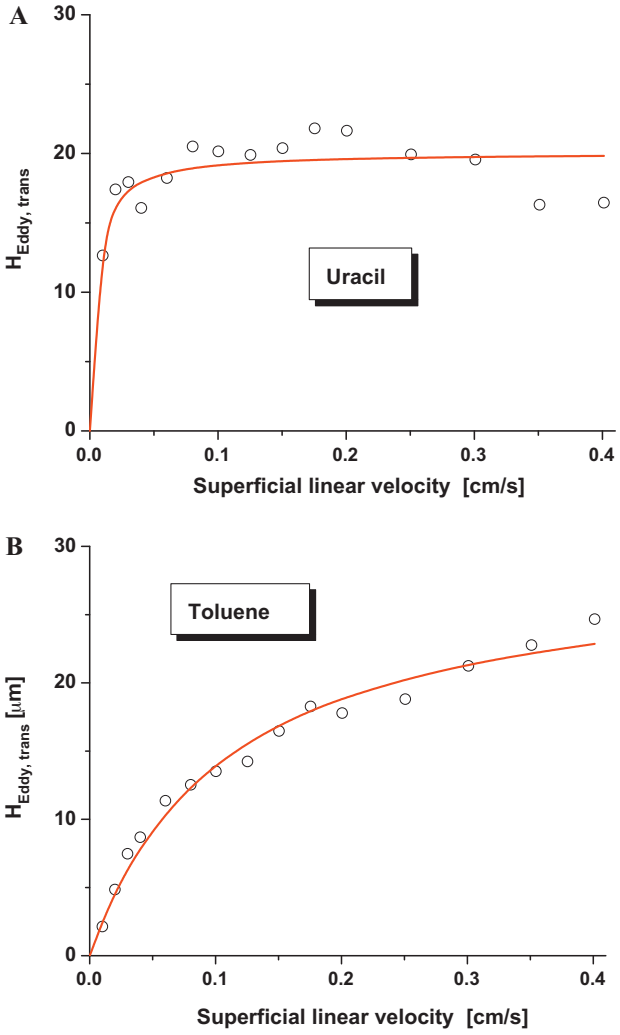

Fig. 7. Comparison between the experimental trans-rod eddy diffusion terms of uracil (A) and toluene (B) and the best theoretical predictions given by Eq. (21). Note the difference between the initial slopes of the plots due to the residence time of toluene being longer than that of uracil.

As mentioned earlier, a relative velocity gradient across a 4.6 mm I.D. monolithic column of the order of 3% was measured across the section of a wide 10 mm I.D. silica rod [13]. Assuming the same value, we can conclude that the persistence-of velocity lengths are 2.2 and 3.5 cm for uracil and toluene, respectively. In other words, the molecules entering the center of the monolithic rod would need to travel a few centimeters along the column to sample the range of velocities that exist across the column. This shows that, in monolithic columns, radial mixing is poor; this may be compounded by a less than perfect distribution at column inlet, collection at the outlet of the sample band. This explains the poor efficiency of the 2.5 cm long column in Fig. 4A. For column longer than 2.5 cm, radial mixing becomes effective, which explains the striking efficiency improvement from Fig. 4A to Fig. 4B and C. Regarding the diffusion parameter ω_α, the lateral diffusion distances required to reach two extreme velocities are about 870 μm and 370 μm for uracil and toluene. This represents about 20 to 50% of the radius of the monolithic rod, which is considerable. For the sake of comparison, this diffusion distance accounts for only 1.7

and 10% of 4.6 and 2.1 mm I.D. columns packed with sub-3 μm shell particles [59].

5. Conclusion

This work analyzes the kinetic performance of a first commercial generation of 4.6 mm I.D. monolithic columns (Onyx), which have average throughpore and skeleton sizes of 2.0 and 0.8 μm, respectively (domain size 2.8 μm). The permeability of these monolithic rods is equivalent to that of conventional columns packed with 8 μm spherical particles. The corrected plate heights of three such monolithic columns (25, 50, and 100 mm long) were accurately measured by numerical integration of the elution peak profiles, which corrects for the impact of the peak tailing on the true efficiency of these columns. The sample diffusion coefficients were actually measured by peak parking experiments with a column packed with solid particles and not estimated from approximate literature correlations.

Surprisingly, the minimum plate height observed was only 17 μm for the most retained compound ($k = 2.6$). Using the peak parking method to measure the longitudinal diffusion HETP term allows the isolation of the contribution of the eddy diffusion HETP term for non-retained and retained compounds. Whereas the column length has no measurable impact on the eddy diffusion of late eluted compounds, it controls the HETP of non-retained samples. This demonstrates that the distribution of the local velocities across the rod is heterogeneous. Because the residence time and the radial dispersion coefficient of analytes increase with increasing retention, the radial velocity gradients are relaxed more efficiently during band migration along the column [53,54].

The relatively poor column efficiency observed (60 000 plates/m maximum) is due to the trans-column distribution of the flow velocities taking place over a few hundred micrometers. This large-scale velocity bias generates HETPs as high as 20 μm at high flow rates and limits the performance of the Onyx monolithic columns. For the sake of comparison, the contributions of the trans-throughpore (distance ≃1 μm) and short-range inter-throughpore (distance of a 3–6 μm) to the overall HETP do not exceed 0.5 and 1.5 μm [15]. Additionally, we showed that it takes a migration distance of 2.5 cm along a 4.6 mm I.D. monolithic column for a compound to move from a slow (column center) to a fast (wall region) velocity streamline by a pure convection.

Due to the very slow rate of radial dispersion, the distribution of the sample band at the inlet of wide bore monolithic columns is of primordial importance. It is definitely important to introduce the sample where the velocity distribution is homogeneous. Unfortunately, we ignore everything about the radial velocity distribution across monolithic rods. Due to poor radial mixing, the simultaneous injection of the sample band at the wall and in the center of the rod could enhance peak tailing and lead to poor apparent column efficiency. Decreasing the domain size is of no help in decreasing the HETP because trans-throughpore and short-range inter-throughpore velocity biases have only a marginal impact on the overall HETP. The development of more efficient 4.6 mm I.D. monolithic columns will be a difficult task which could involve the following steps

- Take a standard 4.6 mm I.D. monolithic rod and measure the flow velocity profile across and along the whole volume of this rod, elaborate a morphology reconstruction of this rod and use flow calculation models to predict accurate velocity distributions. Compare with the results of actual observations. Identify the zones where the flow distribution is uniform.
- Prepare an inlet distributor that will selectively introduce the sample into a zone where the flow velocity distribution is nearly uniform
- Prepare an outlet distributor that will collect directly the eluent from the zone where the local velocity is the smallest in order to compensate for radial velocity gradients. This is of crucial importance with non-retained or poorly retained samples.
- Once these steps provide satisfactory results with 3 μm domain size silica monolith, repeat the same process with smaller domain size for narrow-bore columns (2 mm I.D.).

In conclusion, it seems that research aiming at improving the performance of monolithic columns should adopt the following goals: first, the macroscopic structure of the silica rod should be made more radially homogeneous. This might be easier with 3 than with 4.6 mm I.D. columns. Next, the column inlet and outlet should be optimized to minimize the influence of the residual structure heterogeneity. Finally, the domain size could be reduced to about 2 μm. We hope to have the opportunity to test monolithic columns of the second generation in the near future in order to assess whether further progress were made in the important field of column technology for faster and higher resolution separations, returning competition in a field currently dominated by the sub-2 μm fully porous and sub-3 μm superficially porous particles.

Nomenclature

Roman letters

A	eddy dispersion term (m)
B	longitudinal diffusion coefficient (m^2/s)
C_i	discreet sample concentration in the recorded concentration profile (kg/m^3)
C_{skel}	trans-skeleton mass transfer coefficient (s)
C_f	film mass transfer coefficient defined in Eq. (11) ($m^{1/2}\,s^{1/2}$)
d_p	equivalent particle size (m)
$d_{throughpores}$	average throughpore size (m)
$d_{skel.}$	average monolithic skeleton size (m)
$\overline{D_r}$	average radial dispersion coefficient (m^2/s)
D_{skel}	effective skeleton diffusivity (m^2/s)
D_m	bulk molecular diffusion coefficient (m^2/s)
F_v	flow rate (m^3/s)
H	total column HETP (m)
$H_{Channel}$	trans-throughpore eddy diffusion HETP term (m)
H_{Eddy}	eddy diffusion HETP term (m)
H_{Film}	external film mass transfer resistance term (m)
H_{Flow}	trans-rod eddy diffusion term associated with a pure convective exchange mechanism (m)
$H_{Diffusion}$	trans-rod eddy diffusion term associated with a pure diffusive exchange mechanism (m)
$H_{Long.}$	longitudinal diffusion HETP term (m)
H_{Short}	short-range inter-throughpore eddy diffusion HETP term (m)
$H_{Skel.}$	trans-skeleton mass transfer resistance HETP term (m)
$H_{Trans\text{-}rod}$	trans-rod eddy diffusion HETP term (m)
k	retention factor of non-excluded analytes
k_0	specific permeability (m^2)
K_c	Kozeny–Carman permeability constant
k_f	film mass transfer coefficient (m/s)
L	monolithic column length (m)
ΔP	pressure drop along the monolithic column (Pa)
R_c	monolith column inner radius (m)
T	temperature during the HETP experiments (K)
T_{PP}	temperature during the PP experiments (K)

t_i discreet time variable in the recorded concentration profile (s)
t_R elution time (s)
Δt_p parking residence time (s)
u_S superficial linear velocity (m/s)
$u_{R,PP}$ migration linear velocity during the peak parking experiments (m/s)
$u(x)$ interstitial linear velocity at the reduced radial coordinate x of the rod (m/s)
x reduced radial coordinate to the column inner radius R

Greek letters
δ_0 zone retention factor
ϵ_e external column porosity
ϵ_t total column porosity for non-excluded analytes
ϵ_{skel} skeleton porosity
γ_e external obstructive factor of the monolithic rod
γ_r coefficient in the expression of the convective radial dispersion coefficient
η eluent viscosity (Pa s)
μ_1 experimental first moment in presence of column (s)
$\mu_{1,ex}$ first moment of the extra-column band profiles (column replaced with a zero volume union connector) (s)
μ'_2 experimental second central moment in presence of column (s^2)
$\mu'_{2,ex}$ second central moment of the extra-column band profiles (column replaced with a zero volume union connector) (s^2)
ω_β relative trans-rod velocity bias to the average axial velocity
ω_α reduced radial diffusion length for a trans-rod velocity bias to the skeleton size d_{skel}
ω_λ reduced persistence-of-velocity flow length for a trans-rod velocity bias to the skeleton size d_{skel}
$\Delta\sigma^2_{PP}$ increment of the peak variance in the parking method experiments (s^2)

Acknowledgements

This work was supported in part by the cooperative agreement between the University of Tennessee and the Oak Ridge National Laboratory. We thank Tivadar Farkas (Phenomenex, Torrance, CA, USA) for the gift of the 100 × 4.6 mm column packed with 1.9 μm non-porous particles.

References

[1] K. Nakanishi, N. Soga, J. Am. Ceram. Soc. 74 (1991) 2518.
[2] H. Minakuchi, K. Nakanishi, N. Soga, N. Ishizuka, N. Tanaka, Anal. Chem. 68 (1996) 3498.
[3] K. Cabrera, G. Wieland, D. Lubda, K. Nakanishi, N. Soga, H. Minakuchi, K. Unger, Trends Anal. Chem. 17 (1998) 133.
[4] S. Hjerten, J.-L. Liao, J. Chromatogr. 457 (1988) 165.
[5] F. Svec, J. Frechet, Anal. Chem. 64 (1992) 820.
[6] Q. Wang, F. Svec, J. Frechet, J. Chromatogr. A 669 (1994) 230.
[7] F. Gritti, W. Piatkowski, G. Guiochon, J. Chromatogr. A 978 (2002) 81.
[8] M. Kele, G. Guiochon, J. Chromatogr. A 960 (2002) 19.
[9] F. Gritti, W. Piatkowski, G. Guiochon, J. Chromatogr. A 983 (2003) 51.
[10] K. Cabrera, J. Sep. Sci. 27 (2004) 843.
[11] G. Guiochon, J. Chromatogr. A 1168 (2007) 101.
[12] K. Cabrera, in: Proceedings of the 31st International Symposium on High Performance Liquid Phase Separations and Related Techniques (HPLC-2007), Ghent, Belgium.
[13] K.S. Mriziq, J.A. Abia, Y. Lee, G. Guiochon, J. Chromatogr. A 1193 (2008) 97.
[14] J. Abia, K. Mriziq, G. Guiochon, J. Chromatogr. A 1216 (2009) 3185.
[15] D. Hlushkou, S. Bruns, A. Holtzel, U. Tallarek, Anal. Chem. 82 (2010) 7150.
[16] O. Nunez, K. Nakanishi, N. Tanaka, J. Chromatogr. A 1191 (2008) 231.
[17] R. Hahn, A. Tscheliessnig, P. Bauerhansl, A. Jungbauer, J. Biochem. Biophys. Methods 70 (2007) 87.
[18] D. Hlushkou, S. Bruns, U. Tallarek, J. Chromatogr. A 1217 (2010) 3674.
[19] S. Khirevich, A. Daneyko, A. Holtzel, A. Seidel-Morgenstern, U. Tallarek, J. Chromatogr. A 1217 (2010) 4713.
[20] T. Laiblin, W. Arlt, R. Kaiser, R. Kirsch, Chem. Ing. Tech. 79 (2007) 1213.
[21] Proceedings of the 32nd International Symposium on High Performance Liquid Phase Separations and Related Techniques, Baltimore, MD, May 10–16, 2008.
[22] J.J. DeStefano, T.J. Langlois, J.J. Kirkland, J. Chromatogr. Sci. 46 (2007) 254.
[23] F. Gritti, I. Leonardis, D. Shock, P. Stevenson, A. Shalliker, G. Guiochon, J. Chromatogr. A 1217 (2010) 1589.
[24] F. Gritti, G. Guiochon, J. Chromatogr. A 1217 (2010) 1604.
[25] F. Gritti, I. Leonardis, J. Abia, G. Guiochon, J. Chromatogr. A 1217 (2010) 3219.
[26] G. Guiochon, F. Gritti, J. Chromatogr. A 1218 (2011) 1915.
[27] F. Gritti, G. Guiochon, Chem. Eng. Sci. 65 (2010) 6327.
[28] F. Gritti, G. Guiochon, J. Chromatogr. A (2011).
[29] M. Al-Bokari, D. Cherrak, G. Guiochon, J. Chromatogr. A 975 (2002) 275.
[30] F. Gritti, G. Guiochon, J. Chromatogr. A 1169 (2007) 125.
[31] J. Knox, H. Scott, J. Chromatogr. 282 (1983) 297.
[32] F. Gritti, G. Guiochon, Chem. Eng. Sci. 61 (2006) 7636.
[33] K. Miyabe, Y. Matsumoto, G. Guiochon, Anal. Chem. 79 (2007) 1970.
[34] F. Gritti, G. Guiochon, AIChE J. 57 (2011) 333.
[35] F. Gritti, G. Guiochon, J. Chromatogr. A 1217 (2010) 5137.
[36] F. Gritti, G. Guiochon, J. Chromatogr. A 1218 (2011) 3476.
[37] F. Gritti, G. Guiochon, Chem. Eng. Sci. (2011).
[38] K. Miyabe, G. Guiochon, J. Phys. Chem. B 106 (2002) 8898.
[39] J. Giddings, Dynamics of Chromatography, Marcel Dekker, New York, NY, 1965.
[40] R. Landauer, J. Appl. Phys. 23 (1952) 779.
[41] H. Davis, J. Am. Ceram. Soc. 60 (1977) 499.
[42] F. Gritti, G. Guiochon, AIChE J. 57 (2011) 346.
[43] F. Gritti, G. Guiochon, J. Chromatogr. A 1216 (2009) 4752.
[44] R. Bird, W. Stewart, E. Lightfoot, Transport Phenomena, John Wiley and Sons, New York, NY, 2002.
[45] K. Miyabe, J. Chromatogr. A 1183 (2008) 49.
[46] J.H. Knox, L. McLaren, Anal. Chem. 36 (1964) 1477.
[47] K. Miyabe, N. Ando, G. Guiochon, J. Chromatogr. A 1216 (2009) 4377.
[48] Y. Miyabe, K. Matsumoto, G. Guiochon, Anal. Chem. 65 (2010) 3859.
[49] D. Ludlum, R. Warner, H. Smith, J. Phys. Chem. 66 (1962) 1540.
[50] P. Dunlop, C. Pepela, B. Steel, J. Am. Chem. Soc. 92 (1970) 6743.
[51] C. Wilke, P. Chang, AIChE J. 1 (1955) 264.
[52] J. Li, P. Carr, Anal. Chem. 69 (1997) 2530.
[53] F. Gritti, G. Guiochon, AIChE J. 56 (2010) 1495.
[54] F. Gritti, G. Guiochon, J. Chromatogr. A 1217 (2010) 6350.
[55] F. Gritti, G. Guiochon, J. Chromatogr. A 1217 (2010) 8167.
[56] M. Martin, G. Guiochon, Anal. Chem. 56 (1984) 614.
[57] F. Gritti, M. Martin, G. Guiochon, Anal. Chem. 81 (2009) 3365.
[58] U. Tallarek, E. Bayer, G. Guiochon, J. Am. Chem. Soc. 120 (1998) 1494.
[59] F. Gritti, G. Guiochon, J. Chromatogr. A 1218 (2011) 1592.